Original Article | Open Access

Intelligent Food Systems

Zhao *et al. Intell. Food Syst.* **2026**, *5*, xx **DOI:** 10.20517/ifs.2026.xxx

Damage prediction of transmission lines typhoon disasters considering

Hui Hou[1], Zhiwei Zhang[1], Shiwen Yu[2], Yong Huang[3], Yongxi Zhang[4], Zhaoyang Dong[5]

Keywords:
Typhoon, transmission line, tower-line coupling, two-step reliability model, Weibull distribution, uniform corrosion

Citation: Hou H, Zhang Z, Yu S, Huang Y, Zhang Y, Dong Z. Damage prediction of transmission lines under typhoon disasters considering multi-effect. *Intell. Food Syst.* **2026**, *5*, xx. http://dx.doi.org/10.20517/ifs.2026.xxx

Received: 27 Dec 2020
First Decision: 2 Mar 2021
Revised: 9 Mar 2021
Accepted: 7 May 2021
Online: 27 May 2021

Academic Editor:
Oscar Castillo
Copy Editor:
Yue-Yue Zhang
Production Editor:
Yue-Yue Zhang

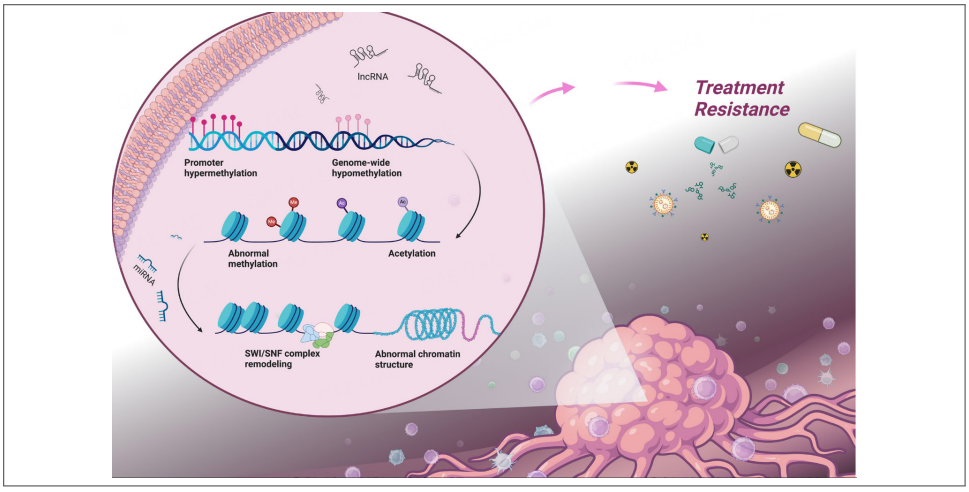

Abstract

Aim: It is necessary to study the resilience of transmission lines under typhoon disasters considering multi-effect, because typhoon disasters pose a great threat to coastal transmission lines and existing research ignored multi-effect and obtained conservative results.

Method: This paper proposes a method to predict the damage of transmission towers under typhoon disasters considering the multi-effect of tower-line coupling, aging, corrosion, guy wire reinforcement, etc. The tower-line coupling effect uses a two-step reliability model. The first step calculates the damage probability of transmission lines. Then, we couple the wind load of transmission lines to towers through binomial distribution. The second step calculates the damage probability of transmission towers. The aging effect uses two-parameter Weibull distribution to calculate the aging failure probability. The corrosion effect uses the uniform corrosion theory to calculate the corrosion failure probability. The guy wire reinforcement is realized by increasing the mean value of design wind load for strength curves.

Check for updates

[1]School of Automation, Wuhan University of Technology, Wuhan 430070, Hubei, China.
[2]Electric and Electronics Engineering, University of Illinois at Chicago, Chicago 60607, USA.
[3]Electric Power Research Institute, Guangdong Power GRID Co. Ltd., Guangzhou 510080, Guangdong, China.
[4]School of Electrical and Information Engineering, Changsha University of Science & Technology, Changsha 410114, Hunan, China.
[5]School of Electrical Engineering and Telecomunications, University of New South Wales, Sydney 2052, Australia.

Correspondence to: Prof. Hui Hou, School of Automation, Wuhan University of Technology, Luoshi Road, Hongshan District, Wuhan 430070, Hubei Province, China. E-mail: 1343395935@whut.edu.cn

Next, this paper uses probability addition equation to integrate multi-effect and obtained the final damage prediction results. Finally, we used the 110-kV THJ (TieHaiJia) line in Guangdong province, China under Typhoon "Mangkhut" in 2018 as an example to check the accuracy of proposed method.

Results: The results show that the comprehensive failure probability is close to 1, and the reinforcement effect can only reduce the failure probability by 0.003.

Conclusion: It is concluded that considering the tower-line coupling effect to improve failure probability is closer to practice, but the reinforcement effect should not be blindly improved.

INTRODUCTION

In recent years, typhoons have caused huge damage to coastal power system in China. On the one hand, a typhoon may damage a large number of electrical equipment and cause difficulties for the stable and reliable operation in power sectors. On the other hand, it can result in power outage for many users and have serious impact on industrial production and citizens's lives. For the purpose of improving the ability to withstand risks in power system, there is a need to study the damage risk of transmission lines under typhoon disasters.

The neighbor of La in the periodic table, Ba, has been thought to be one of the promising host elements for the synthesis of superconducting hydrides [3]. At ambient pressure, the *Pnma* BaH_2 (BaH_2-I) is the thermodynamical stable phase of barium hydride. Heating at ambient pressure can drive a structural transition of BaH_2 from the low-symmetry *Pnma* to the high-symmetry Ni_2In-type structure with the space group $P6_3/mmc$ (BaH_2-II). This structure transition makes BaH_2 be one of the prominent ionic conductors with potential applications in energy storage because the high-symmetry phase exhibits a hydrogen ion conductivity of 0.2 $S{\cdot}cm^{-1}$ at 630°C that is an order of magnitude larger than that of state-of-the-art oxide ion conductors [22]. However, both BaH_2-I and BaH_2-II are not good candidates for superconductivity because they are semiconductors with a wide band gap around 1.9~2.9 eV [16]. The high-pressure experiments [13,19] suggest that BaH_2 undergoes successive phase transformations: BaH_2-I first converts to BaH_2-II at around 2.5 GPa, then transforms to AlB_2-type simple hexagonal BaH_2-III accompanied by a closure of the band gap at around 57 GPa. Although BaH_2-III is metallic, superconductivity has not been observed.

Chen et al studied barium hydrides at higher pressures ranging from 75 to 173 GPa and reported several hydrogen-rich barium hydrides [3]. In particular, their transport measurements revealed the onset of superconductivity at 20 K and 140 GPa in BaH_{12} with a pseudocubic face-centered cubic Ba sublattice. This superconducting hydride is suggested to be a unique molecular hydride because it contains H_2 and H_3^{-1} molecular units, forming separate flat H_{12} chains, which are rarely observed in the high-symmetry clathrate superhyrdies at high pressures. In hydrides with H_2 and H_3^{-1} molecular units, the H-H bond disrupts the delocalized metallic bonding network, and their covalent nature may reduce the interaction between the vibrational modes of hydrogen atoms and the electronic states of the host lattice, which can lead to weaker electron-phonon coupling. Several recent studies have shown that the presence of hydrogen molecules generally form more insulating states than metallic states [6,7]. Therefore, the molecular hydrogen units are generally not beneficial for superconductivity and high T_c.

Based on the networking value model and the statistics of hundreds of superconducting hydrides, an earlier study by one of the authors suggests that stretching the H-H bond or elimination of the hydrogen molecular units can favor superconductivity [2]. Guided by this quantitative rule, in our study, we design new ternary barium hydrides that show higher T_c than BaH_{12} at lower pressures. Aiming at eliminating or reducing the number of H_2 and H_3^{-1} molecular units in barium hydride, we introduce four elements with light atomic mass (Li, Be, B

and C) to barium hydride and perform high-throughput crystal structure screening to locate the low-enthalpy structures up to 200 GPa. By studying the structural and electronic properties of a series of low-lying ternary barium hydride, we find that H_2 molecular units remain widely observed in these ternary barium hydrides, while H_3^{-1} is almost absent. Due to the universal existence of molecular units in the studied ternary hydrides, more insulating states than metallic states are found in the low-enthalpy structure space. Although metallic states were much fewer than the semiconducting or insulating phases, there are several metallic molecular hydrides showing interesting properties. In particular, $BeBaH_4$ with tetragonal structure is nearly thermodynamically stable at 100 GPa and can be still dynamically stable at 50 GPa. In addition, by combining the quick estimator of superconducting T_c based on the networking value model[2,17] with the ab initio methods, $BeBaH_8$ with orthorhombic structure has been predicted to be superconducting with a T_c of 49 K at 100 GPa. The value of T_c can be further boosted by improving the pressure, reaching 107 K at 200 GPa. This $BeBaH_8$ remains dynamically stable down to 15 GPa although it is not superconducting due to the substantial reduction of the electron-phonon coupling constant.

This paper proposes a method to predict the damage of transmission towers under typhoon disasters considering multi-effect. The highlights of this paper are:

- We propose a theoretical solution to the tower-line coupling effect from the perspective of probability. Compared with wind tunnel experiment, the obtained probability is close to complete failure.

- We consider the effects of aging, corrosion and guy wire reinforcement to improve calculation accuracy closer to the engineering practice.

- We verify the significant contribution of the tower-line coupling effect to the comprehensive damage probability, and the improvement of reinforcement effect has little impact on reducing the former.

The rest of this paper is organized as follows. Section 2 uses a two-step reliability model to calculate the wind load of transmission lines. Section 3 discusses the damage calculation principles under three effects of corrosion, aging and guy wire reinforcement. Finally, in Section 4, we draw a conclusion.

PHYSICAL MODEL FOR WIND LOAD OF TRANSMISSION LINES

Figure 1 is the structure diagram of damage prediction method considering multi-effect. It shows the calculation principle in this and the next section. In Section 2, we first calculate the wind load of conductors and towers and calculate the failure probability of conductors through interference area method in structural reliability theory[18]. Then, we use binomial distribution to couple the wind load of conductors to towers and calculate the damage probability of towers. In Section 3, we use probability addition equation[19] to integrate multi-effect and tower-line coupling effect.

METHODS

Crystal structure prediction

The crystal structure prediction methods, i.e., the particle swarm algorithm implemented in CALYPSO[23,24] and the evolutionary algorithm implemented in CrySPY[26], were used to predict the crystal structures of A-Ba-H (A = Li, Be, B and C) at pressures up to 200 GPa. The crystal structure prediction was performed with a fixed composition, and cell sizes were explored up to 32 atoms per cell. A total of around 100,000 structures were screened during the crystal structure prediction. The enthalpy and forces of the predicted crystal structures were calculated by first-principles density functional theory (DFT) methods. The DFT calculations were carried out

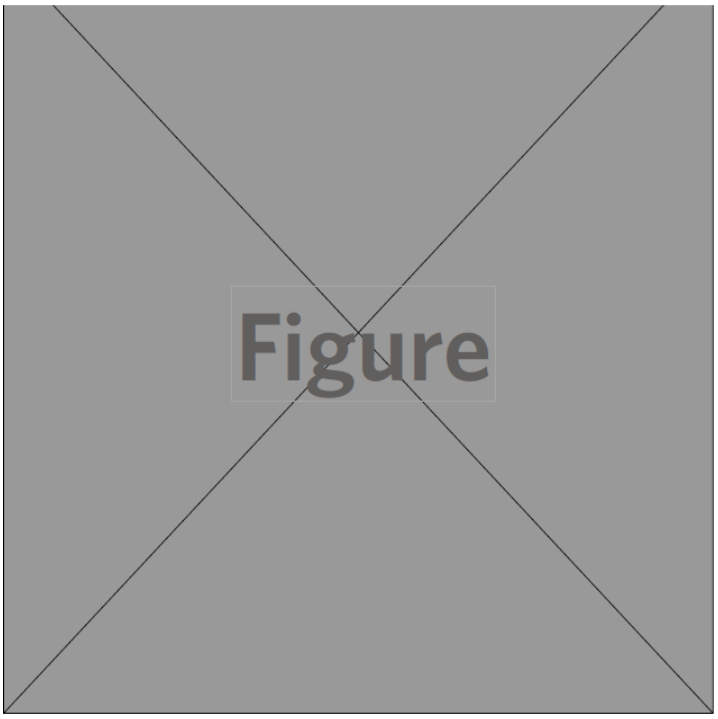

Figure 1. The structure diagram of damage prediction method considering multi-effect.

using the Vienna Ab initio Simulation Package (VASP)[14,15] employing the projector-augmented wave (PAW) method. The exchange-correlation functional was treated in the generalized gradient approximation within the parameterization of Perdew, Burke, and Ernzerhof[18]. To generate k-points for different crystal structures during structure screening, we employed the k-point generation scheme in Pymatgen[11], using a grid density of 100 k-points per Å^{-3} of reciprocal cell volume. An energy cutoff of 450 eV was used in the crystal structure prediction. To construct the convex hull phase diagram, we considered all materials available in our crystal structure prediction, as well as those we could find from the Materials Project[12]. The structures were fully optimized until the energy convergence criterion of 10^{-8} eV and force criterion of 10^{-3} eV·Å^{-1} were satisfied.

Electronic structure calculations

In high-throughput DFT calculations of the density of states (DOS), we used the Gaussian smearing method in VASP. To ensure accurate results, we used a narrow smearing width of 0.05 eV accompanied by a dense k point grid with 200 points per Å^{-3} of reciprocal cell volume. To extract the total DOS and the element/orbital projected DOS, we used the Sumo[8] code. In both band and phonon dispersion calculations, the special k-path were generated using Sumo[8]. To estimate the superconducting critical temperature T_c based on the networking value model, we used the TcESTIME code[2,17]. The value of T_c with an error of 60 K is correlated to Φ_{DOS}:

$$T_c = (750\Phi_{DOS} - 85)\ \text{K}, \tag{1}$$

$$\Phi_{DOS} = \phi H_f H_{DOS}^{-3} \tag{2}$$

where ϕ is the networking value based on the electron localization function, H_f is the hydrogen fraction, and H_{DOS} is the hydrogen fraction of the total DOS at the Fermi energy.

Phonon and electron-phonon coupling calculations

The phonon, and electron-phonon coupling properties were investigated using density-functional perturbation theory (DFPT) method implemented in Quantum Espresso[10,9]. The dynamical stability was also cross-checked

by the supercell and finite displacement methods implemented in Phonopy[20]. The Quantum Espresso calculations were performed using norm-conserving pseudopotentials from the strict set of PseudoDojo[21]. In Quantum Espresso calculations, geometry optimizations were carried out using uniform Γ-centered k-point grids with a density of 3000 k-points. In the electron-phonon coupling calculations, the k-grid from the structure relaxation was doubled in each direction as the coarse grid. In addition, and it was further quadrupled in each direction as the fine grid. In the particular case of $BeBaH_8$, the results converged well with a k-grid of $42 \times 42 \times 42$. The critical temperature for superconductivity was calculated using the Allen-Dynes formula:

$$T_c = \frac{f_1 f_2 \omega_{\log}}{1.20} \exp\left(\frac{-1.04(1+\lambda)}{\lambda - \mu^*(1+0.62\lambda)}\right), \tag{3}$$

$$f_1 = \left(1 + \left(\frac{\lambda}{2.46(1+3.8\mu^*)}\right)^{3/2}\right)^{1/3}, \tag{4}$$

$$f_2 = \left(1 + \frac{\lambda^2\left(\frac{\bar{\omega}_2}{\omega_{\log}} - 1\right)}{\lambda^2 + [1.82(1+6.3\mu^*)(\frac{\bar{\omega}_2}{\omega_{\log}})]^2}\right), \tag{5}$$

where f_1 and f_2 are correction factor depending on the electron-coupling constant λ, Coulomb pseudopotential parameter μ^*, average logarithm frequency $\omega_{\log}$, and $\bar{\omega}_2$. The frequencies $\bar{\omega}_n$ are the nth root of the nth moment of the normalized distribution $g(\omega) = \frac{2}{\lambda\omega}\alpha^2 F(\omega)$[25]. In our study, the Coulomb pseudopotential parameter (μ^*) of 0.1 was used.

RESULTS

A_2BaH_{12} at 200 GPa where A = Li, Be, B, and C

Chen *et al.* reported the molecular hydride BaH_{12} exhibited a T_c of 20 K at 140 GPa experimentally[3]. To investigate the effect of the introduced light-mass elements (A = Li, Be, B, and C) on BaH_{12} at high pressures, we first performed crystal structure prediction of 2 formula units A_2BaH_{12} (i.e. 30-atom $A_4Ba_2H_{24}$) at 200 GPa. In each crystal structure prediction, we carried out around 20-50 generations for each fixed stoichiometry, with each generation including 100 crystal structures. For each stoichiometry of A_2BaH_{12}, the structural and electronic properties of the twenty low-lying states are studied. The space group and enthalpy of the low-lying structures for $LiBaH_{12}$, $BeBaH_{12}$, $BBaH_{12}$ and $CBaH_{12}$ are shown in Supplementary Table 1, Table 2, Table 3 and Table 4, respectively. The crystal structures of the lowest-enthalpy states at 200 GPa, as predicted by our crystal structure calculations, are shown in.

Because the 2 f.u. A_2BaH_{12} is a large cell and most predicted structures show low symmetry (most of them being $P1$ without any symmetry operation except identity operation), it is computationally demanding to carry out an high-throughput calculation of T_c using DFPT methods implemented in Quantum Espresso. Alternatively, we note that the networking value model[2,17] has been widely recognized and used in many recent studies to predict superconducting critical temperatures[5,1,4]. Because the networking value model is based on electron localization functions that can be obtained in standard ab initio calculations, it makes the estimation of T_c much computationally cheaper compared to the direct computation from solving Eliashberg spectral functions in DFPT calculations. Previously, the networking value model was applied into the high-throughput calculation of T_c and guided the theoretical discovery of the 100 K superconductivity in $Lu_4H_{11}N$ and the near-room-temperature superconductivity in binary LuH_6 and LuH_{10}[6].

By using the networking value model method implemented in TcESTIME[2], we calculated the critical temperatures for the low-lying metallic structures of the 30-atom A_2BaH_{12} at 200 GPa. The values obtained are shown in the Supplementary Tables 1~4. The highest T_c for Li_2BaH_{12} is 56 K while no superconducting phase is observed in C_2BaH_{12}. Both $BeBaH_{12}$ and $BBaH_{12}$ show critical temperatures above 70 K which approach the boiling point of liquid nitrogen.

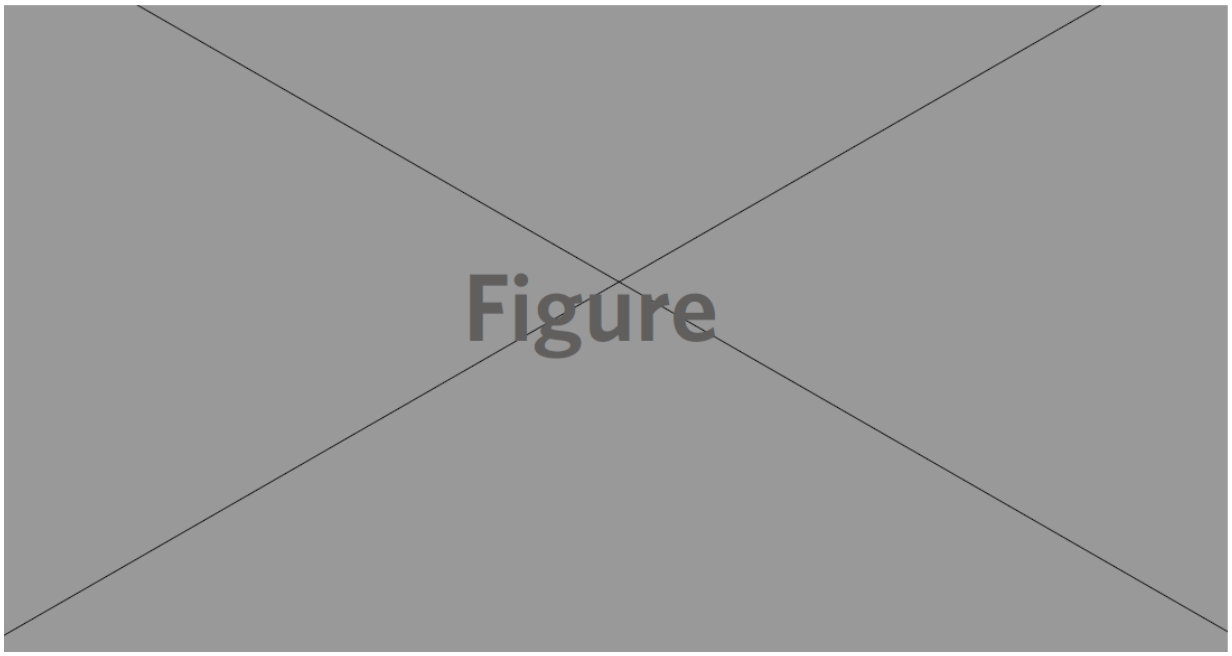

Figure 2. The track of strong typhoon "Mangkhut" and distribution of THJ line.

In examining B_2BaH_{12} and C_2BaH_{12}, we note from Supplementary Tables 1–4 that more than half of the structures among the twenty low-enthalpy states exhibit insulating character. Relatively, more low-lying structures of Li_2BaH_{12} and Be_2BaH_{12} show metallic conductivity. The analysis of these low-lying structures of $ABaH_{12}$ at 200 GPa demonstrates that the introduction of Li and Be into the barium hydrides has more possibilities to form metallic properties than B and C. In particular, the lowest-lying structures of $P4bm$ B_2BaH_{12} and $P1$ C_2BaH_{12}, illustrated in in are both insulating, whereas the lowest-lying states of Cc Li_2BaH_{12} and $Cmmm$ Be_2BaH_{12} are both metallic. Although the lowest-lying structures of Li_2BaH_{12} and Be_2BaH_{12} are metals, the minimal interatomic distances in show that their minimal H-H bond lengths are 0.830 and 0.756 Å, respectively, which is just slightly larger than the minimal H-H bond lengths in B_2BaH_{12} and C_2BaH_{12}. Therefore, the H_2 molecule units are present in all the ground-state structures of $ABaH_{12}$. However, unlike the other three cases but like the $Cmc2_1$ BaH_{12} reported by Chen et al[3], the H-H-H (H_3^{-1}) chain is only observed in Li_2BaH_{12}, as illustrated in(a).

PREDICTION RESULTS OF FAILURE PROBABILITY CONSIDERING MULTI-EFFECT

Overview of typhoon "Mangkhut"

On the afternoon of 7 September 2018, No. 22 Typhoon "Mangkhut" was generated in the Northwest Pacific Ocean. After shifting into the northeastern corner of the South China Sea on the morning of 15 September, it suddenly shifted westward, hitting the Pearl River Delta head-on and seriously affecting Guangdong province. "Mangkhut" had the widest impact area on land, the longest impact time of strong wind and the maximum gust speed among all typhoons that have landed in Guangdong province in history. This case studied selected the 110-kV THJ line, a typical line with a running time of 12 years. Figure 2 shows the typhoon path and the location of the THJ line.

Prediction result

When calculating wind load, the uneven coefficient of wind pressure takes 0.75; the adjustment coefficient of wind load on towers is 1; the windward area of towers is 5 m2; the outer diameter of lines is 0.0096 m; the span is 250 m. The height variation coefficient of wind pressure is 1; and the shape coefficient of wind load is 1.2.

Table 1. Probability definition considering multi-effect

Multi-effect	Reinforcement effect	Tower-line coupling effect	Aging effect (P_5)	Corrosion effect (P_6)
Reinforcement effect				
Tower-line coupling effect				
Aging effect (P_5)				
Corrosion effect (P_6)				

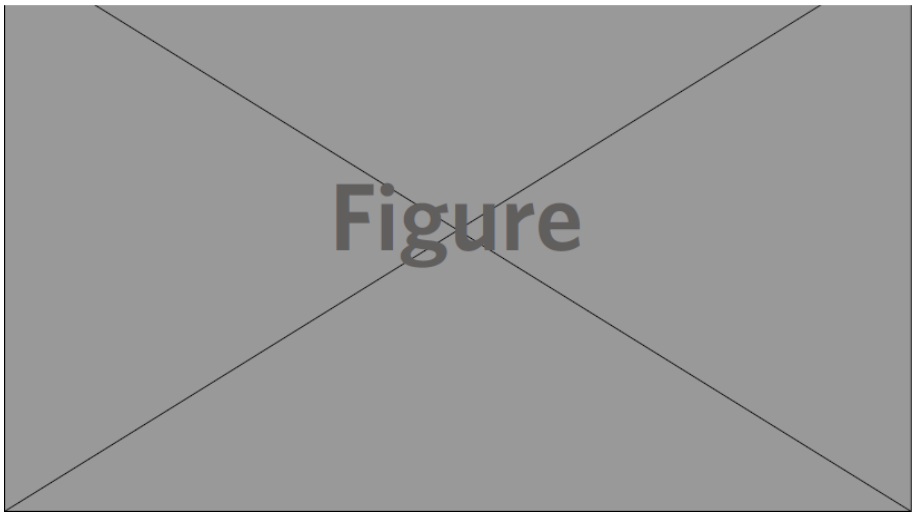

Figure 3. Damage probability of THJ line in 10 cases.

Both two-step reliability calculations use the 3-s average instantaneous wind speed, which makes the predicted results more conservative and is conducive to more comprehensive prevention work.

Figure 3 shows the trend of predicted damage probability from 61 towers of THJ line under typhoon "Mangkhut", while Supplementary Table 2 shows the specific damage probability value.

$BeBaH_x$ at pressures

Given that the analysis at 200 GPa indicates that the incorporation of Be and Li into Ba-H promotes the formation of more metallic states compared to B and C, and that T_c is expected to be higher for Be than for Li, we further investigated $BeBaH_x$ ($x = 2n, \quad n \in \{1, 2, 3, \ldots, 12\}$). However, we shifted our focus to explore the structures at 100 GPa to identify potential superconducting Be-Ba-H compounds that could be stabilized at pressures lower than those experimentally reported for barium hydrides.[3]. Figure shows the phase diagram at 100 GPa based on the crystal structures from our crystal structure prediction and Materials Project database[12]. We find the $BeBaH_6$ and $BeBaH_{18}$ are on the convex hull, which implies that they are thermodynamically stable. However, they are both semiconductors.

Although we did not find any thermodynamically stable $BeBaH_x$ compounds that are metallic, we identified several metallic stoichiometries lying within 100 meV/atom from the convex hull. In particular, by estimating T_c using the networking value model, we find that two hydrides, $BeBaH_4$ and $BeBaH_8$, may be superconducting with T_c higher than 25 K (± 60 K). These two hydrides $BeBaH_4$ and $BeBaH_8$ are 11 meV/atom and 36 meV/atom above the convex hull, respectively at 100 GPa. Since these two compounds are not far from the convex hull, implying the feasibility of experimental synthesis, the electron-phonon coupling properties of these two structures were further investigated using DFPT method.

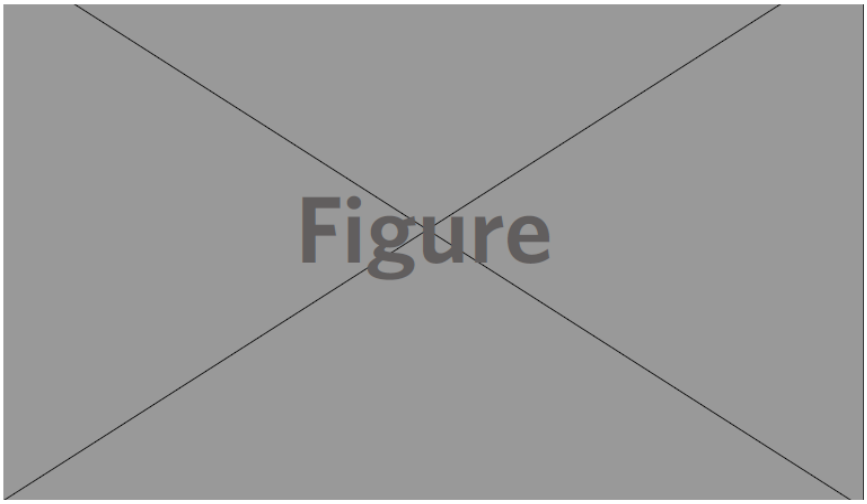

Figure 4. Four cases with the highest damage probability of THJ line.

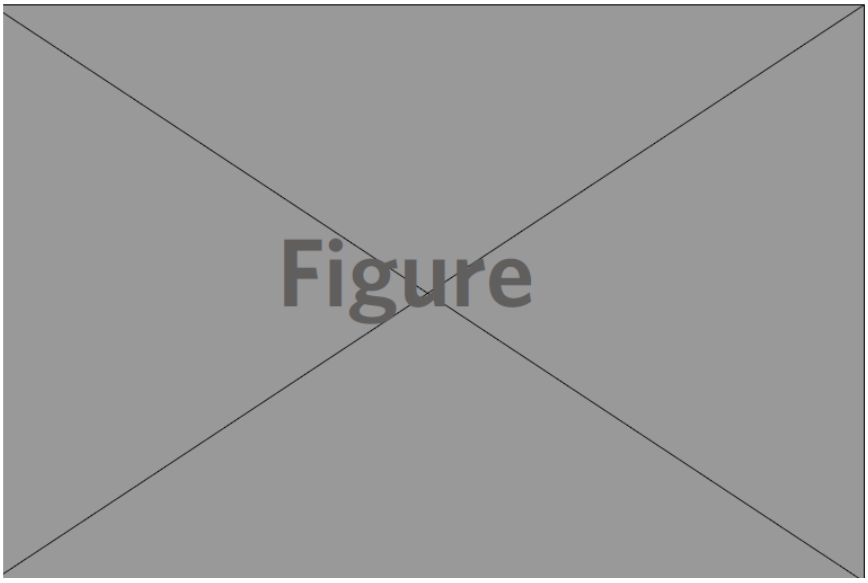

Figure 5. Failure probability without considering the tower-line coupling effect.

The hydride $BeBaH_4$ has a tetragonal crystal structure and a space group of $P4/mmm$ (No. 123) at 100 GPa, in which a = 2.91 Å and c = 3.87 Å. The crystal structure is shown in. At 100 GPa, the phonon spectrum in shows that this $P4/mmm$ $BeBaH_4$ is dynamically stable. However, because of the small electron-phonon coupling constant λ of 0.15, the Allen-Dynes formula predicts that it is not a superconductor at 100 GPa. We find that a higher pressure of 200 GPa does not help to develop superconductivity because the value of λ is only slightly increased to 0.16. Despite the absence of superconductivity, this tetragonal $BeBaH_4$ can be stabilized at a lower pressure of 50 GPa. By comparing the phonon spectra at 50 and 100 GPa, we can find that the decreased pressure only has a small effect on the low-energy phonon modes consisting of heavy atoms Be and Ba, but in the meantime it softens the high-energy hydrogen modes significantly.

The crystal structure of $BeBaH_8$ has an orthorhombic Bravais lattice and a space group of $Cmc2_1$ (No. 36). There are two formula units in the primitive cell, resulting in 20 atoms in the primitive cell. The primitive cell of

$BeBaH_8$ is shown schematically in. At 100 GPa, the electronic band structure and the density of sates in suggest that $BeBaH_8$ is metallically conductive. There are two bands crossing the Fermi level, forming one electron pocket at Y and one hole pocket at Γ. More importantly, the electronic states at the Fermi level are dominated by hydrogen atoms with minor contributions from the heavy host metals Ba and Be, signaling that $BeBaH_8$ may be a hydride superconductor. The phonon dispersions and phonon density of states (PDOS) do not show any imaginary mode, indicating that $BeBaH_8$ is dynamically stable at 100 GPa. Furthermore, we find that $BeBaH_8$ remains dynamically stable in the harmonic approximation at pressures down to only 15 GPa, as evidenced by the phonon bands and PDOS shown in (b). However, the electronic band structure and DOS in (b) show that $BeBaH_8$ enters into the semiconducting state, exhibiting an indirect band gap of 1.5 eV.

By solving the Eliashberg spectral function $\alpha^2F(\omega)$, the electron-phonon coupling constant of $BeBaH_8$ is calculated to be around 0.8 at 100 GPa. The corresponding Eliashberg spectral function $\alpha^2F(\omega)$ and the cumulative frequency-dependent electron-phonon function $\lambda(\omega)$ are shown in. By comparing the $\alpha^2F(\omega)$ and the phonon density of states in, we find that the electron-phonon coupling is dominated by the phonon modes of H and Be character ranging from 10 THz to 40 THz, followed by the minor contribution of phonon modes of Ba below 10 THz. Using Allen-Dynes equation with Coulomb pseudopotential parameter (μ^*) of a typical value 0.1, the value of T_c is around 49 K. Upon increasing pressure, we find that the electron-phonon coupling can be enhanced significantly. The Eliashberg spectral functions $\alpha^2F(\omega)$ of 150 GPa and 200 GPa are compared to that at 100 GPa in. Due to the overall softening of the high-frequency pure H modes, these modes join to contribute additional electron-phonon coupling at 150 and 200 GPa, compared to the case of 100 GPa in which the high-frequency pure H modes almost have negligible contributions to λ. As a result, the values of T_c are increased to 73 K and 107 K at 150 GPa and 200 GPa, respectively.

CONCLUSIONS

This study took the wind load model of transmission conductors and towers as the research object and simulated the tower-line coupling effect through the two-step reliability model. This model can reflect the physical essence of tower-line coupling effect in principle. This paper establishes an aging failure model based on two-parameter Weibull distribution, a corrosion failure model based on uniform corrosion theory and a guy wire reinforcement model based on reliability theory. Finally, this paper uses probability addition equation to integrate multi-effect and establishes a damage prediction model for transmission lines under typhoon disasters. The prediction model was verified by taking the 110-kV THJ line, a typical line in Guangdong province, China, under Typhoon "Mangkhut" in 2018, as an example.

However, this paper buildes the damage prediction model of transmission tower-line system considering multi-effect under typhoon disasters only through the physical strength-stress interference model and does not use data mining or intelligent algorithms to analyze historical data for probability prediction. In addition, since the reinforcement effect does not significantly inhibit the tower-line coupling effect, this paper does not explore the design wind speed standard that should be achieved after guy wire reinforcement. The results show that tower-line coupling effects, aging effects, corrosion effects and the influence of guy wire reinforcement play important roles in the failure probability calculation of transmission equipment under typhoon disasters. The method with four effects considered can effectively improve the prediction accuracy.

DECLARATIONS

Acknowledgments

The measurement and recording of the experimental data in this paper was done with the strong support of the staff from Electric Power Research Institute of Guangdong Power Grid Co., Ltd., and I would like to express my heartfelt thanks to them.

Authors' contributions

Funding acquisition, project administration, provide research resources, and supervision: Hou H
Methodology, software, and writing-review editing: Zhang Z
Data process, investigation, Methodology, software, visualization and writing-original draft: Yu S
Conceptualization, data acquisition, project supervision, and validation: Huang Y
Writing-review editing: Hou H, Zhang Y, Dong Z

Availability of data and materials

The data is obtained from Guangdong Electric Power Research Institute, the author will not be shared and explain it.

Financial support and sponsorship

This work is supported by University-Industry Collaborative Education Program of Ministry of Education of the People's Republic of China (201902056044).

Conflicts of interest

All authors declared that there are no conflicts of interest.

REFERENCES

1. Bai Z, Bhullar M, Akinpelu A, Yao Y. Unveiling future superconductors through machine learning. *Materials Today Physics* 2024; 43:101384.
2. Belli F, Novoa T, Contreras-García J, Errea I. Strong correlation between electronic bonding network and critical temperature in hydrogen-based superconductors. *Nat Commun* 2021;12:1748.
3. Chen W, Semenok DV, Kvashnin AG, Huang X, Kruglov IA, Galasso M, Song H, Duan D, Goncharov AF, Prakapenka VB, Oganov AR, Cui T. Synthesis of molecular metallic barium superhydride: pseudocubic BaH12. *Nat Commun* 2021;12:331.
4. Denchfield A, Park H, Hemley RJ. Designing multicomponent hydrides with potential high Tc superconductivity, 2024.
5. Denchfield A, Park H, Hemley RJ. Electronic structure of nitrogen-doped lutetium hydrides. *Phys. Rev. Mater.* 2024;8:L021801.
6. Fang YW, Đorđe Dangić, Errea I. Assessing the feasibility of near-ambient conditions superconductivity in the Lu-N-H system, 2023.
7. Ferreira PP, Conway LJ, Cucciari A, Di Cataldo S, Giannessi F, Kogler E, Eleno LTF, Pickard CJ, Heil C, Boeri L. Search for ambient superconductivity in the Lu-N-H system. *Nat. Commun.* 2023;14:244.
8. Ganose AM, Jackson AJ, Scanlon DO. sumo: Command-line tools for plotting and analysis of periodic *ab initio* calculations. *Journal of Open Source Software* 2018;3:717.
9. Giannozzi P, Andreussi O, Brumme T, Bunau O, Nardelli MB, Calandra M, Car R, Cavazzoni C, Ceresoli D, Cococcioni M, Colonna N, Carnimeo I, Corso AD, de Gironcoli S, Delugas P, Jr RAD, Ferretti A, Floris A, Fratesi G, Fugallo G, Gebauer R, Gerstmann U, Giustino F, Gorni T, Jia J, Kawamura M, Ko HY, Kokalj A, Küçükbenli E, Lazzeri M, Marsili M, Marzari N, Mauri F, Nguyen NL, Nguyen HV, de-la Roza AO, Paulatto L, Poncé S, Rocca D, Sabatini R, Santra B, Schlipf M, Seitsonen AP, Smogunov A, Timrov I, Thonhauser T, Umari P, Vast N, Wu X, Baroni S. Advanced capabilities for materials modelling with QUANTUM ESPRESSO. *Journal of Physics: Condensed Matter* 2017;29:465901.
10. Giannozzi P, Baroni S, Bonini N, Calandra M, Car R, Cavazzoni C, Ceresoli D, Chiarotti GL, Cococcioni M, Dabo I, Dal Corso A, de Gironcoli S, Fabris S, Fratesi G, Gebauer R, Gerstmann U, Gougoussis C, Kokalj A, Lazzeri M, Martin-Samos L, Marzari N, Mauri F, Mazzarello R, Paolini S, Pasquarello A, Paulatto L, Sbraccia C, Scandolo S, Sclauzero G, Seitsonen AP, Smogunov A, Umari P, Wentzcovitch RM. QUANTUM ESPRESSO: a modular and open-source software project for quantum simulations of materials. *Journal of Physics: Condensed Matter* 2009;21:395502 (19pp).
11. Jain A, Hautier G, Moore CJ, Ping Ong S, Fischer CC, Mueller T, Persson KA, Ceder G. A high-throughput infrastructure for density functional theory calculations. *Computational Materials Science* 2011;50:2295–2310.
12. Jain A, Ong SP, Hautier G, Chen W, Richards WD, Dacek S, Cholia S, Gunter D, Skinner D, Ceder G, Persson KA. Commentary: The Materials Project: A materials genome approach to accelerating materials innovation. *APL Materials* 2013;1:011002.
13. Kinoshita K, Nishimura M, Akahama Y, Kawamura H. Pressure-induced phase transition of BaH2 : Post Ni2In phase. *Solid State Communications* 2007;141:69–72.
14. Kresse G, Furthmüller J. Efficient iterative schemes for ab initio total-energy calculations using a plane-wave basis set. *Phys. Rev. B* 1996; 54:11169–11186.
15. Kresse G, Furthmüller J. Efficiency of ab-initio total energy calculations for metals and semiconductors using a plane-wave basis set. *Computational Materials Science* 1996;6:15–50.

16. Luo W, Ahuja R. Ab initio prediction of high-pressure structural phase transition in BaH2. *Journal of Alloys and Compounds* 2007; 446-447:405–408. Proceedings of the International Symposium on Metal-Hydrogen Systems, Fundamentals and Applications (MH2006)
17. Novoa T, di Mauro ME, Inostroza D, El Haloui K, Sisourat N, Maday Y, Contreras-García J. TcESTIME: predicting high-temperature hydrogen-based superconductors. *Chem. Sci.* 2024;–.
18. Perdew JP, Burke K, Ernzerhof M. Generalized Gradient Approximation Made Simple. *Phys. Rev. Lett.* 1996;77:3865–3868.
19. Shuttleworth HA, Osmond I, Strain C, Binns J, Buhot J, Friedemann S, Howie RT, Gregoryanz E, Peña Alvarez M. Pressure-Induced Metallization of BaH and the Effect of Hydrogenation. *J. Phys. Chem. Lett.* 2023;14:11490–11496.
20. Togo A, Tanaka I. First principles phonon calculations in materials science. *Scripta Materialia* 2015;108:1–5.
21. van Setten M, Giantomassi M, Bousquet E, Verstraete M, Hamann D, Gonze X, Rignanese GM. The PseudoDojo: Training and grading a 85 element optimized norm-conserving pseudopotential table. *Comput. Phys. Commun.* 2018;226:39–54.
22. Verbraeken MC, Cheung C, Suard E, Irvine JTS. High H– ionic conductivity in barium hydride. *Nature Mater* 2015;14:95–100.
23. Wang Y, Lv J, Zhu L, Ma Y. Crystal structure prediction via particle-swarm optimization. *Phys. Rev. B* 2010;82:094116.
24. Wang Y, Lv J, Zhu L, Ma Y. CALYPSO: A method for crystal structure prediction. *Computer Physics Communications* 2012;183:2063–2070.
25. Xie SR, Quan Y, Hire AC, Deng B, DeStefano JM, Salinas I, Shah US, Fanfarillo L, Lim J, Kim J, Stewart GR, Hamlin JJ, Hirschfeld PJ, Hennig RG. Machine learning of superconducting critical temperature from Eliashberg theory. *npj Comput Mater* 2022;8:074502.
26. Yamashita T, Kanehira S, Sato N, Kino H, Terayama K, Sawahata H, Sato T, Utsuno F, Tsuda K, Miyake T, Oguchi T. CrySPY: a crystal structure prediction tool accelerated by machine learning. *Science and Technology of Advanced Materials: Methods* 2021;1:87–97.

Disclaimer/Publisher's Note: All statements, opinions, and data contained in this publication are solely those of the individual author(s) and contributor(s) and do not necessarily reflect those of OAE and/or the editor(s). OAE and/or the editor(s) disclaim any responsibility for harm to persons or property resulting from the use of any ideas, methods, instructions, or products mentioned in the content.

© The Author(s) 2021. **Open Access** This article is licensed under a Creative Commons Attribution 4.0 International License (https://creativecommons.org/licenses/by/4.0/), which permits unrestricted use, sharing, adaptation, distribution and repro-duction in any medium or format, for any purpose, even commercially, as long as you give appropriate credit to the original author(s) and the source, provide a link to the Creative Commons license, and indicate if changes were made.